INSTITUTE OF PHYSICS PUBLISHING NONLINEARITY

Nonlinearity **19** (2006) 2813–2831 doi:10.1088/0951-7715/19/12/005

Linear stability of a ridge

J R King[1], **A Münch**[2,3] **and B Wagner**[3]

[1] Theoretical Mechanics Section, School of Mathematical Sciences, University of Nottingham, Nottingham NG7 2RD, UK
[2] Institute of Mathematics, Humboldt University of Berlin, 10099 Berlin, Germany
[3] Weierstrass Institute for Applied Analysis and Stochastics (WIAS), 10117 Berlin, Germany

E-mail: John.King@nottingham.ac.uk, muench@mathematik.hu-berlin.de and wagnerb@wias-berlin.de

Received 14 September 2005, in final form 27 August 2006
Published 2 November 2006
Online at stacks.iop.org/Non/19/2813

Recommended by M P Brenner

Abstract

We investigate the stability of the three-phase contact line of a thin liquid ridge on a hydrophobic substrate for flow driven by surface tension and van der Waals forces. We study the role of slippage in the emerging instability at the three-phase contact line by comparing the lubrication models for no-slip and slip conditions at the liquid/substrate interface.

For both cases we derive a sharp-interface model via matched asymptotic expansions and derive the eigenvalues from a linear stability analysis of the respective reduced models. We compare our asymptotic results with the eigenvalues obtained numerically for the full lubrication models.

Mathematics Subject Classification: 76M45, 34B15, 65M06

PACS numbers: 68.15.+e

1. Introduction

In this paper we investigate a contact-line instability, which occurs when a thin liquid film dewets a substrate and the liquid/substrate interface condition allows for large slippage.

In the past decades, contact-line instabilities have been considered for thin liquid films that *wet* a solid substrate, both theoretically and experimentally. These instabilities are typically driven by forces such as gravity [1–5], Marangoni stresses or both [6–10]. The modelling dimension-reduced lubrication models, which are derived from the underlying Navier–Stokes equations, typically employ a slip boundary condition or a precursor model to regularize the stress singularity at the three-phase contact line, whereby the height of the precursor or the slip length are usually much smaller than the height of the actual wetting film. The choice of the boundary condition at the three-phase contact line typically enters only weakly and does not significantly influence the eventual appearance of fingers, see for example [3, 9, 11, 12].

 © 2006 IOP Publishing Ltd and London Mathematical Society Printed in the UK

In contrast to these previous investigations, the dewetting scenarios we consider here concern film heights that are typically orders of magnitude smaller. The physical background is described by a thin viscous polymer film that is uniformly spread on a substrate, such as a silicon wafer with a hydrophobic coating, which typically consists of a monolayer of grafted brushes. For such a multi-layered system one can reconstruct the disjoining pressure from a corresponding intermolecular potential, which is composed of attractive long-range van der Waals contributions and a short-range term which accounts for Born-type repulsion, see, e.g. [13, 14]. The latter term provides a cut-off by penalizing a thinning of the film below a positive thickness threshold given by the minimum of the potential. In such a situation the thin film dewets in a process that is initiated either spontaneously through spinodal decomposition or is induced, for example, through nucleation. The dry spots, or holes, that form as a result subsequently grow as the newly formed contact line recedes, thereby accumulating liquid in a characteristic capillary ridge at the edge of the hole, which increases in width and height as the dewetting proceeds. In a variety of experimental situations it is observed that, while in some cases the growth of the hole continues until it collides with neighbouring holes, in others the ridge of the hole destabilizes into finger-like structures, eventually pinching off to form droplets. Such a finger-like contact-line instability has also been observed for straight (as opposed to radially-symmetric) dewetting ridges, see [15–21]. Since this instability will influence the evolution of the dewetting process and the emerging dewetting patterns, it is important to understand the underlying mechanism, whereby in particular these fingers, which would otherwise result in stationary ridges of fluid being left behind in the near-dry region behind the dewetting front, destabilize and break up into droplets.

Some of the first theoretical studies were done in [22–25], where the dewetting rate and shape of the ridge were treated using approximate formulae derived from scaling arguments and energy balances. In [22] it was found that in the case of large slippage the dewetting proceeds according to a $t^{2/3}$ law for the evolution of the dewetting rim in contrast to the nearly linear law for the no-slip situation. It was argued in [26] that due to this dewetting rate, thicker portions (introduced via small perturbations) of the dewetting rim move more slowly than thinner ones, leading to the appearance and growth of fingers. This idea for a mechanism for the contact-line instability in the nanofluidic regime was taken up by [27, 28], where the evolution of the film surface $z = h(x, y, t)$ was modelled via a lubrication approximation that includes the influence of surface tension, the intermolecular potential $\phi(h)$ and a condition for large slip at the solid/liquid interface, where we note that, within the described physical context, slippage is understood as *effective* (sometimes also called *apparent*) slippage. Moreover, let us note that the same mechanism that leads to the appearance of fingers should take effect during the process of their eventual pinch-off from the receding front, since the thicker portions of the fingers will stay behind.

In order to introduce the lubrication models we will investigate here, we choose coordinates so that x, y denote directions parallel to the (planar) substrate and z the direction normal to it. The pressure at $z = h(x, y, t)$ is given to leading order in the lubrication approximation by

$$p = -\Delta h + \phi'(h), \tag{1.1}$$

where $\phi'(h)$ is the first derivative of the intermolecular potential with respect to the liquid film thickness h. A typical choice for $\phi(h)$, and the one we will adopt in this paper, is (see [13])

$$\phi'(h) = \varepsilon^{-1}\Phi'(h/\varepsilon), \qquad \text{where } \Phi(v) = \frac{1}{8v^8} - \frac{1}{2v^2}. \tag{1.2}$$

Note that $\Phi'(1) = 0$ and $\Phi''(1) > 0$, so that ϕ has a minimum at $h = \varepsilon \ll 1$; the reason for incorporating the dependences upon ε embodied by (1.2) will become clear in sections 3 and 4. It implies that very thin films with a thickness scale of ε are energetically preferred to thicker

films, and the latter therefore tend to dewet. Making use of the length-scale separation in the x, y versus z directions, one can then derive the lubrication model from the Navier–Stokes equations in conjunction with conservation of mass, (1.1) and appropriate boundary conditions at the free surface and at the solid/liquid interface, namely,

$$h_t + \nabla \cdot [h^n \nabla(\Delta h - \phi'(h))] = 0, \tag{1.3}$$

stated here (as are all equations in this paper) in non-dimensional form. For a detailed derivation and scaling analysis of a family of lubrication approximations that include large slippage, we refer to [29]. The exponent n depends on the boundary condition at the solid/liquid interface. A widely used condition relates the slippage velocity u of the liquid at the wall to the local shear rate u_z via Navier-slip condition

$$u = b\, u_z \qquad \text{at } z = 0, \tag{1.4}$$

where the slip length parameter b corresponds to the distance below the substrate at which the liquid velocity extrapolates to zero. For the above slip boundary condition, the no-slip condition is obtained if $b = 0$, corresponding to the mobility h^3. For large b one can show (see, e.g. [29]) that the mobility is h^2, which we will call here the slip case. In [30] it could be shown numerically that the contact-line evolves according to a $t^{2/3}$ law in contrast to the no-slip case, where a linear law was found with a weak logarithmic correction, confirming the results by [22]; see also [31] who investigated the no-slip case. In [27] a linear stability analysis showed that small perturbations of the receding rim are amplified and by orders of magnitude larger in the slip case than in the no-slip one. Moreover, while the perturbations of the contour lines become very symmetrical with respect to the maximum of the ridge in the no-slip case, they are asymmetrical in the slip regime. Moreover, in [28] it was shown via numerical simulations that these properties carry over into the nonlinear dynamics of the perturbations. We remark at this point that for the physical applications described above, the contact angles of the dewetting rims may become as large as 60°, which may render a lubrication approximation questionable there. For this reason the fully nonlinear curvature was included in the treatment (see, e.g. [27, 30]), showing qualitatively the same results.

The purpose of this paper is to present a careful asymptotic treatment with respect to this instability by comparing linear stability results for the lubrication models with mobilities h^3 (corresponding to the no-slip case) and h^2 (corresponding to the slip case). A first asymptotic study of the stability of a moving ridge for mobility h^3 was performed in [32], where asymptotic solutions for the shape of the dewetting ridges, their dewetting rates and their contact-line instability were derived. In [33] a variational formulation was used to obtain a free boundary problem for the contact line for the no-slip situation, and a stability analysis of the contact-line motion was performed in [34].

We pursue our comparisons of the stability properties of the no-slip and slip cases by considering the simplest situation of the evolution of a perturbed stationary ridge. The study of this case has the advantage that the sharp-interface models, that we derive from the lubrication models via matched asymptotic expansions, turn out to be simple enough to enable in some cases the derivation of the dispersion relation in analytic form and allow direct comparison with our numerical results. We remark that while we shall take the ridge to be straight, the analysis can be generalized to curved ones.

We begin our analysis by first studying the stability of the ridge numerically in section 2. In sections 3 and 4 we derive the sharp-interface models and the corresponding dispersion relations and compare them with our numerical findings.

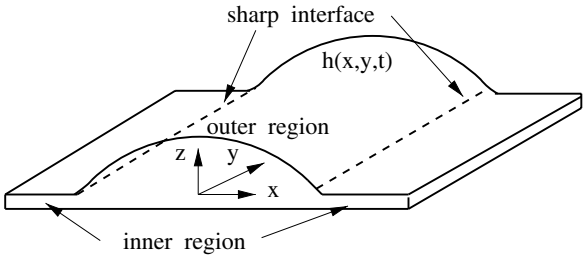

Figure 1. Sketch of the initial state of the ridge.

2. Stationary ridges and their stability

In this section we study numerically the contact-line instability of a stationary ridge that initially extends to $\pm\infty$ in the y-direction and is symmetrical about zero in the x-direction and assumes the (small) equilibrium height εh_∞ for $x \to \pm\infty$, see figure 1.

We thus begin with the lubrication model (1.3), (1.2), together with the boundary conditions

$$\lim_{x\to\pm\infty} h(x, y, t) = \varepsilon h_\infty. \tag{2.1}$$

From (1.3), (2.1), the ridge profiles can readily be found by dropping all terms with derivatives in t and y and integrating the resulting ODE. The constants of integration are determined by the far-field conditions, and we obtain, after two integrations,

$$h_x = \pm 2^{1/2}[\phi(h) - \phi(\varepsilon h_\infty) - \phi'(\varepsilon h_\infty)(h - \varepsilon h_\infty)]^{1/2}. \tag{2.2}$$

The plus sign applies for the left side of the ridge and the minus sign for the right. We assume in our scalings that the cross-sectional area of the fluid in the ridge is such that its maximum is one (without losing generality, since this can always be achieved by rescaling the equation with $h_{\max}$ and redefining ε). This assumption implies that the right-hand side of (2.2) must be zero for $h = 1$, i.e. we must observe the constraint

$$\phi(1) - \phi(\varepsilon h_\infty) - \phi'(\varepsilon h_\infty)(1 - \varepsilon h_\infty) = 0. \tag{2.3}$$

This fixes h_∞ for a given ε (on which ϕ depends). One easily finds for (1.2) that $h_\infty \sim 1+\varepsilon/16$ as $\varepsilon \to 0$. Note that $h_\infty = 1 + O(\varepsilon)$ holds more generally as long as $\phi'(\varepsilon) = 0$. Profiles for the ridges for different values of ε are shown in figure 2; note that the base states do not depend on the mobility h^n and hence are the same for the no-slip and slip cases.

Next we probe the stability of these equilibrium solutions with respect to disturbances in the y-direction via the normal modes ansatz

$$h(x, y, t) = h_0(x) + \beta h_1(x; k)\mathrm{e}^{\mathrm{i}ky+\sigma t}, \qquad \text{where } 0 < \beta \ll 1$$

and $h_0(x)$ is the previously found ridge profile. Introducing this into (1.3) and (2.1) we obtain the $O(\beta)$ problem

$$\sigma h_1 + \partial_x[h_0^n \partial_x(h_{1xx} - k^2 h_1 - \phi''(h_0)h_1)] - k^2 h_0^n(h_{1xx} - k^2 h_1 - \phi''(h_0)h_1) = 0 \tag{2.4}$$

and

$$\lim_{x\to\pm\infty} h_1(x; k) = 0. \tag{2.5}$$

The eigenvalue problem (2.4), (2.5) was solved on a sufficiently large, finite domain using a standard finite-difference discretization scheme and inverse vector iteration to calculate the

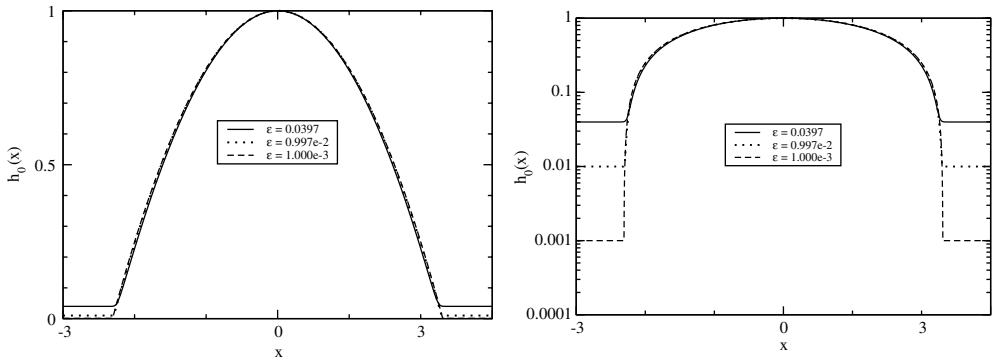

Figure 2. The ridge profiles for different values of ε. On the right side, the axis for h_0 has been scaled logarithmically to enlarge the thin profiles beyond the 'contact lines'.

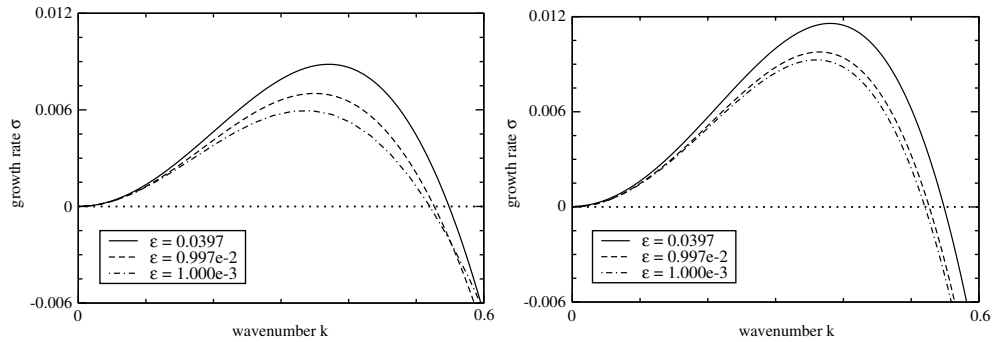

Figure 3. The growth rates for the (unstable for $0 < k < k_c$) peristaltic mode for different values of ε, for the no-slip case $n = 3$ (left) and for the slip case $n = 2$ (right).

two eigenvalues with the largest real part, for a range of wavenumbers k. It turns out that both eigenvalues are real. One is negative for all $k > 0$ while the other is positive for all non-zero wave-numbers below a certain cut-off value k_c and negative $k > k_c$. This unstable one is a peristaltic mode, whereby the sinusoidal perturbations of the contact lines on each side of the ridge are out of phase by half a wavelength. The other, i.e. stable, eigenvalue corresponds to perturbations that are in phase, i.e. are zig–zag modes. Both families are needed in order to generate a complete set of eigenmodes; we shall limit ourselves to investigating the first member of each, conjecturing that these are the ones most likely to exhibit instabilities. It is worth noting that in the absence of a Sturm–Liouville theory for such fourth-order problems, the stability of the first mode of one of either of the two families would not *a priori* guarantee the stability of the first member of the other, so it is essential that both be investigated. Details of the results can be found in figure 3 for the peristaltic and in figure 4 for the zig–zag mode.

Note that the eigenvalues do (of course) depend on the mobility, i.e. on the value of n. In figure 3 the wavelength of the unstable mode and its growth rate are slightly larger for the slip than for the no-slip case, while the cut-off (neutrally-stable) wavenumbers k_c are quite close. The difference is even more dramatic for the zig–zag mode, where the eigenvalue for the slip case is about twice that for no-slip.

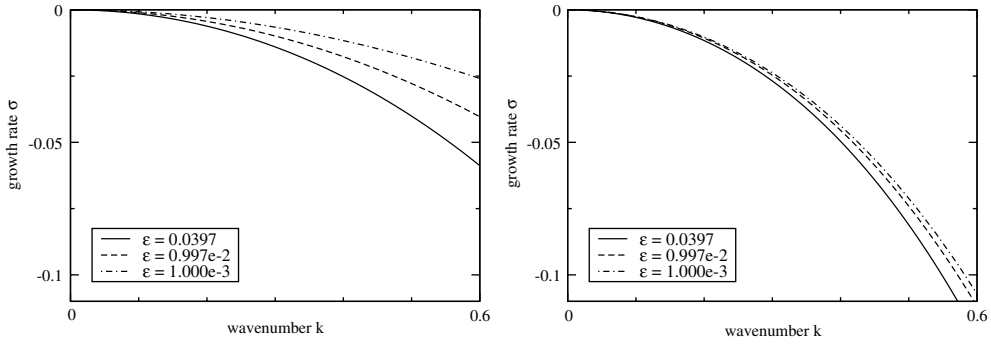

Figure 4. The (negative) growth rates for the (stable) zig–zag mode for different values of ε, for the no-slip case (left) and for the slip case (right).

3. Sharp-interface model for the slip-dominated case

3.1. Derivation of the model

Outer problem. We start from equation (1.3) for $n = 2$, i.e.

$$h_t + \nabla \cdot [h^2 \nabla (\triangle h - \varepsilon^{-1} \Phi'(h/\varepsilon))] = 0, \tag{3.1}$$

and the far-field conditions

$$\lim_{x \to \pm\infty} h(x, y, t) = \varepsilon h_\infty; \tag{3.2}$$

recall that h_∞ satisfies (2.3) and is of $O(1)$.

Transformation to inner coordinates near the contact line. Let $\boldsymbol{x} = (x, y)$ be a point in the neighbourhood of the contact line, which we parametrize by $\boldsymbol{r}(t, s) = (r_1(t, s), r_2(t, s))$, where s denotes arclength. Then

$$\boldsymbol{x} = \boldsymbol{r}(t, s) + \varepsilon \chi \boldsymbol{\nu}(t, s) \tag{3.3}$$

defines the boundary layer with $\chi = O(1)$, which henceforth denotes the 'inner' variable. Note that for an infinite ridge we have two disjoint boundary layers, located around the contact lines Γ^- and Γ^+ on each side of the ridge; hence, we have two parameter functions $\boldsymbol{r}(t, s)$ and two pairs of normal and tangent vectors. Where necessary, these will be distinguished by adding a superscript + or −.

The normal vectors are defined to point into the domain Ω occupied by the ridge, and the unit tangent vectors are chosen so that they form a right-hand system with the normal vector, i.e. $\det(\boldsymbol{t}, \boldsymbol{\nu}) > 0$. Therefore, $\boldsymbol{t}^-$ points downwards and $\boldsymbol{t}^+$ upwards, as depicted in figure 5. The parametrizations of the boundary curves are assumed to be consistent with this orientation, so that the derivative with respect to the parameter points in the direction of the tangent vector, that is, $\boldsymbol{t}(t, s) = (r_{1s}(t, s), r_{2s}(t, s))$, and by implication, $\boldsymbol{\nu}(t, s) = (-r_{2s}(t, s), r_{1s}(t, s))$. Also by implication of the above, we obtain $r_{2s}(t, s) < 0$ or > 0 on Γ^- or Γ^+, respectively. The curvature κ is defined in the usual way, see (A.3) in appendix A.

In the inner region the height is much less than one, the appropriate scaling being

$$h = \varepsilon v. \tag{3.4}$$

Making use of appendix A we obtain the expression

$$\nabla \cdot (h^2 \nabla p) \sim v^2 p_{\chi\chi}, \tag{3.5}$$

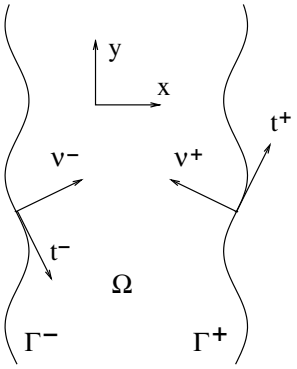

Figure 5. Sketch of a top view of a (perturbed) ridge in the setting of the sharp-interface model, showing the domain Ω occupied by the 'outer' ridge and the tangent and normal vectors to the contact lines that form the boundary of Ω.

where

$$p \sim -\varepsilon^{-1} v_{\chi\chi} + \varepsilon^{-1}\Phi'(v). \tag{3.6}$$

Hence, to leading order in ε the second term of (3.1) is

$$\varepsilon^{-1}[v^2(v_{\chi\chi} - \Phi'(v))_\chi]_\chi. \tag{3.7}$$

Since the first term of (3.1) is transformed to

$$h_t \sim -V^\nu v_\chi, \tag{3.8}$$

where we denote the tangential velocity and normal velocities by

$$V^t = \boldsymbol{x}_t \cdot \boldsymbol{t}, \qquad V^\nu = \boldsymbol{x}_t \cdot \boldsymbol{\nu}, \tag{3.9}$$

the leading-order inner problem becomes

$$[v^2(v_{\chi\chi} - \Phi'(v))_\chi]_\chi = 0 \tag{3.10}$$

together with the boundary conditions

$$\lim_{\chi\to-\infty} v = 1, \qquad \lim_{\chi\to-\infty} v_\chi = 0, \qquad \lim_{\chi\to-\infty} v_{\chi\chi} = 0. \tag{3.11}$$

Integrating (3.11) twice, using the fact that the potential $\Phi'(1) = 0$, since Φ has a minimum there, we get $v_{\chi\chi} = \Phi'(v)$, hence

$$v_\chi = 2^{1/2}(\Phi(v) - \Phi(1))^{1/2}. \tag{3.12}$$

For matching we need the behaviour for large χ, which is

$$v_\chi \to 2^{1/2}(-\Phi(1))^{1/2} \equiv \lambda \qquad \text{as } \chi \to \infty, \tag{3.13}$$

where the constant λ corresponds to the macroscopic contact angle. For future reference, we remark that for the specific potential (1.2), the numerical value for λ is 0.8660. Transformation of $v \sim \chi\lambda$ back into outer variables via $\chi = ((\boldsymbol{x} - \boldsymbol{r}) \cdot \boldsymbol{\nu})/\varepsilon$ yields

$$h \sim (\boldsymbol{x} - \boldsymbol{r}) \cdot \boldsymbol{\nu}\lambda. \tag{3.14}$$

The following sharp-interface model then results as the leading-order outer problem, together with the boundary condition found by matching to (3.14),

$$h_t = -\nabla \cdot (h^2 \nabla \triangle h) \qquad \text{in } \Omega, \tag{3.15}$$

$$\frac{\partial h}{\partial \nu} = \lambda, \qquad h = 0, \qquad h^2 \frac{\partial}{\partial \nu} \triangle h = 0 \qquad \text{on } \Gamma^-, \tag{3.16}$$

$$\frac{\partial h}{\partial \nu} = \lambda, \qquad h = 0, \qquad h^2 \frac{\partial}{\partial \nu} \triangle h = 0 \qquad \text{on } \Gamma^+, \tag{3.17}$$

where the third boundary condition in (3.16) and (3.17) arises by letting $\chi \to \infty$, $v \to \infty$ in (3.10).

For subsequent discussion on the sharp interface model, it is convenient to introduce an alternative parametrization of the boundary curves Γ^-, Γ^+ as graphs of functions of $s^-(y,t)$ and $s^+(y,t)$, respectively. Specifically, the properly oriented parametrizations are $(s^-(-y,t), -y)$ for Γ^- and $(s^+(y,t), y)$ for Γ^+. The resulting expressions for the tangent and outward-normal vector are

$$\boldsymbol{t}^- = \frac{(-s_y^-, -1)}{((s_y^-)^2+1)^{1/2}} \qquad \text{and} \qquad \boldsymbol{\nu}^- = \frac{(1, -s_y^-)}{((s_y^-)^2+1)^{1/2}}, \tag{3.18}$$

on Γ^-, and

$$\boldsymbol{t}^+ = \frac{(s_y^+, 1)}{((s_y^+)^2+1)^{1/2}} \qquad \text{and} \qquad \boldsymbol{\nu}^+ = \frac{(-1, s_y^+)}{((s_y^+)^2+1)^{1/2}}. \tag{3.19}$$

on Γ^+.

3.2. Stationary-ridge solution

We now assume that the base state is not dependent on t and y, so that it is determined by the boundary value problem

$$(h^2 p_x)_x = 0 \qquad \text{with } p = -h_{xx}, \tag{3.20}$$

$$\frac{\partial h}{\partial \nu} = h_x = \lambda, \qquad h = 0 \qquad h^2 h_{xxx} = 0 \qquad \text{on } s^-, \tag{3.21}$$

$$\frac{\partial h}{\partial \nu} = -h_x = \lambda \qquad h = 0 \qquad h^2 h_{xxx} = 0 \qquad \text{on } s^+. \tag{3.22}$$

Integrating (3.20) twice and using the third (mass-conservation) boundary conditions in (3.21) and (3.22) we find that $h_{xx} = -c$. Integrating this twice and using the first two boundary conditions in (3.21) and (3.22) we get

$$h = \tfrac{1}{2}c(x - s^-)(s^+ - x) \qquad \text{and} \quad c(s^- - s^+) = -2\lambda. \tag{3.23}$$

Transforming the coordinate system again by setting $s^+ = s_0$ and $s^- = -s_0$, we obtain the base state in the simplified form

$$h_0 = \tfrac{1}{2}c(s_0^2 - x^2) \qquad \text{and} \qquad cs_0 = \lambda. \tag{3.24}$$

If we again normalize by choosing $\max h_0 = 1$ then we obtain

$$s_0 = \frac{2}{\lambda} \qquad \text{and} \qquad c = \frac{\lambda^2}{2}. \tag{3.25}$$

3.3. Linear stability

We now investigate the linear stability of the base solution of the previous subsection. Let

$$s^\pm = \pm s_0 + \beta s_1^\pm(y,t), \qquad p = c + \beta p_1(x,y,t), \qquad h = h_0 + \beta h_1(x,y,t). \tag{3.26}$$

At $O(\beta)$ we get

$$h_{1t} = (h_0^2 p_{1x})_x + h_0^2 p_{1yy} \qquad \text{with } p_1 = -h_{1xx} - h_{1yy} \tag{3.27}$$

and the boundary conditions

$$h_{1x} = \frac{\lambda^2}{2} s_1^\pm \qquad \text{at } x = \pm s_0, \tag{3.28}$$

$$h_1 = \pm\lambda\, s_1^\pm \qquad \text{at } x = \pm s_0, \tag{3.29}$$

$$h_0^2 h_{1xxx} = 0 \qquad \text{at } x = \pm s_0\,. \tag{3.30}$$

We make the usual ansatz

$$[s_1^{\pm}(y,t),\, p_1(x,y,t),\, h_1(x,y,t)] = [\hat{s}^{\pm},\, \hat{p}(x),\, \hat{h}(x)]\mathrm{e}^{\sigma t + \mathrm{i}ky} \tag{3.31}$$

and obtain from (3.27)–(3.30) and variable transformation

$$\xi = \frac{\lambda}{2}x, \qquad \tilde{k} = \frac{2}{\lambda}k, \qquad \tilde{\sigma} = \frac{16}{\lambda^4}\sigma, \qquad \tilde{s}_0 = \frac{\lambda}{2}s_0 \tag{3.32}$$

the eigenvalue problem

$$\tilde{\sigma}\hat{h} = -(h_0^2(\hat{h}_{\xi\xi} - \tilde{k}^2\hat{h})_\xi)_\xi + \tilde{k}^2 h_0^2(\hat{h}_{\xi\xi} - \tilde{k}^2\hat{h}), \tag{3.33}$$

$$\hat{h}_\xi = \pm\hat{h} \qquad \text{at } \xi = \pm 1, \tag{3.34}$$

$$0 = h_0^2\hat{h}_{\xi\xi\xi} \qquad \text{at } \xi = \pm 1, \tag{3.35}$$

where

$$h_0 = 1 - \xi^2. \tag{3.36}$$

The ODE (3.33) has regular singular points at the boundary, i.e. at $\xi = \pm 1$. The formulation is symmetric in ξ, so the discussion on the behaviour of the general solution at $\xi = \pm 1$ can be done jointly for both points by setting $\zeta = \xi + 1$ and $\zeta = 1 - \xi$ for the left and right point, respectively. This maps the boundary points to zero and yields the ODE (dropping the $\hat{}$'s and $\sim$'s)

$$h_{\zeta\zeta\zeta\zeta} + \frac{4(1-\zeta)}{\zeta(2-\zeta)}h_{\zeta\zeta\zeta} - 2k^2 h_{\zeta\zeta} - k^2\frac{4(1-\zeta)}{\zeta(2-\zeta)}h_\zeta + \left(\frac{\sigma}{\zeta^2(2-\zeta)^2} + k^4\right)h = 0. \tag{3.37}$$

The general solution is given by $h(\zeta) = \sum_{i=1}^{4} C_i h_i(\zeta)$, where the expansions of the first two basis functions h_i are given at $\zeta = 0$ by the Taylor expansions

$$h_1(\zeta) = \zeta^2 + O(\zeta^4), \qquad h_2(\zeta) = \zeta + O(\zeta^3). \tag{3.38}$$

The expansions for the remaining two basis functions are

$$h_3(\zeta) = 1 + O(\zeta^4), \qquad h_4(\zeta) = \zeta\ln(\zeta) + O(\zeta^2\ln(\zeta)) \tag{3.39}$$

if $\sigma = 0$. Otherwise, the expansion for h_3 becomes

$$h_3(\zeta) = 1 + O(\zeta^2\ln(\zeta)), \tag{3.40}$$

i.e. additional logarithmic terms appear in the higher order corrections. Note that here only h_3 in (3.39) is a Taylor expansion, while logarithms otherwise appear in the expansions for h_3 and h_4. In fact, h_4 is too singular to satisfy the boundary conditions (3.35), which in terms of ζ require $\zeta^2 h_{\zeta\zeta\zeta} \to 0$ at $\zeta \to 0$. Thus we must set $C_4 = 0$. The other boundary condition (3.34) requires $h_\zeta + h \to 0$, from which we get the condition $C_2 + C_3 = 0$. In any case, this amounts to two conditions that are imposed on the general solution at each end of the interval, as required for a fourth-order boundary value problem.

We solved the eigenvalue problem (3.33)–(3.36), using a finite difference/vector iteration scheme, and compared the first two eigenvalues with those obtained for the full model in section 2, both being real for both models. The comparison is shown in figure 6, in terms of the wavenumber k and eigenvalue σ used in (3.31). It can be clearly seen that the eigenvalues for the full problem rapidly converge to the sharp-interface results as $\varepsilon \to 0$.

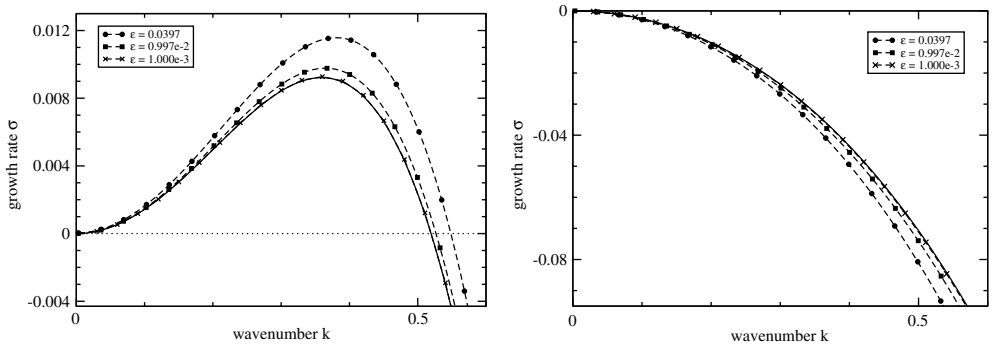

Figure 6. The top first eigenvalue (left) having even eigenfunction and the second eigenvalue (right) having odd eigenfunction, for the slip-dominated case. The results for the asymptotic model obtained from (3.32) to (3.36) are shown by a solid line, the results for the full model shown by dashed lines with symbols.

4. Sharp-interface model for the no-slip situation

4.1. Derivation of the model

Outer problem. We start from equation (1.3) for $n = 3$, i.e.

$$h_t + \nabla \cdot [h^3 \nabla (\triangle h - \varepsilon^{-1} \Phi'(h/\varepsilon))] = 0, \tag{4.1}$$

and far-field conditions

$$\lim_{x \to \pm\infty} h(x, y, t) = \varepsilon h_\infty; \tag{4.2}$$

recall that h_∞ satisfies (2.3) and is of $O(1)$. To capture the instability we transform to the appropriate slow time scale via the logarithmic time dilatation

$$\tau = \delta t, \qquad \delta := \frac{1}{\ln(1/\varepsilon)}, \tag{4.3}$$

which is different from the time scaling for the slip case.

One may wonder where exactly the ansatz used for the slip case fails in the no-slip situation. It turns out that, on following the same procedure, one finally obtains an eigenvalue problem for which the two of the basis functions have to be excluded from the solution, because they are too singular to satisfy conditions (3.34) and the analogue of (3.35). The former condition imposes a further restriction on the combination of the remaining two basis functions, so that altogether the eigenvalue problem has three conditions on each boundary and is hence overdetermined.

The reasons for the differences in the scalings of the slip and no-slip cases relate to the status of the latter as a borderline case separating different regimes of front propagation for the thin-film equation. Such properties are delineated in a more general (but more abstract) context in [35]; see also [32]. Thus, the slip case lies in the moving-front regime of [35], while the no-slip case lies just (this being reflected in the logarithmic scalings) in the fixed-front regime, i.e. the contact-line position must be fixed on an $O(1)$ time scale as $\epsilon \to 0$. Hence, we must assume either small deviations from the contact-line position of the unperturbed ridge, of order $O(\delta)$, or allow the contact-line ridge to evolve on a stretched time scale $O(1/\delta)$. It turns out that for the former choice of scalings, the evolution of the ridge decouples to leading order from the contact-line dynamics; that is, the perturbation of the contact-line appears only in one of the boundary conditions of the resulting eigenvalue problem. In effect, the eigenvalue

problem is the same as obtained for perturbations of a ridge on a fixed domain and can easily be shown to yield stability—i.e. all modes decay. In contrast, the latter choice of scalings preserves the coupling of the contact-line and ridge evolution. We will see below that the resulting eigenvalue problem does, in fact, have unstable modes.

Making use now of (4.3), equation (4.1) becomes

$$\delta h_\tau + \nabla \cdot [h^3 \nabla (\triangle h - \varepsilon^{-1} \Phi'(h/\varepsilon))] = 0. \tag{4.4}$$

Note, that this can also be written as

$$\delta h_\tau - \nabla \cdot (h^3 \nabla p) = 0, \qquad \text{where } p = -\triangle h + \varepsilon^{-1} \Phi'(h/\varepsilon). \tag{4.5}$$

We therefore have in outer coordinates to leading order the quasi-steady equation

$$\nabla \cdot \left(h^3 \nabla p\right) = 0, \qquad \text{where } p = -\triangle h. \tag{4.6}$$

Transformation to inner coordinates near contact line. As in section 3, the boundary layer is defined by (3.3) and v by (3.4). Making use again of appendix A we obtain the expression

$$\nabla \cdot (h^3 \nabla p) \sim \varepsilon v^3 p_{\chi\chi} \tag{4.7}$$

and for p the same leading order terms (of order $O(\varepsilon^{-1})$) as in (3.6). The first term of (4.5) is transformed to

$$\delta h_\tau \sim -\delta V^\nu v_\chi. \tag{4.8}$$

Hence, to leading order, the inner problem reduces to

$$[v^3 (v_{\chi\chi} - \Phi'(v))_\chi]_\chi = 0 \tag{4.9}$$

with

$$\lim_{\chi \to -\infty} v = 1, \qquad \lim_{\chi \to -\infty} v_\chi = 0, \qquad \lim_{\chi \to -\infty} v_{\chi\chi} = 0 \tag{4.10}$$

which is the same as in section 3 and hence (3.12) and (3.13) result for the solution here, too.

Transition layer. In order to be able to match, we here need an additional transition layer. The layer that properly connects outer and inner layers is found by setting

$$\zeta = \delta V^\nu \ln \chi, \qquad v = \chi \varphi(\zeta), \tag{4.11}$$

see [36] for details. Substitution of this into (4.7) and (4.8) we obtain the leading-order problem, assuming $1 - \zeta / V^\nu > 0$,

$$\varphi + \varphi^3 \varphi_\zeta = 0 \tag{4.12}$$

with solution

$$\varphi \sim (K - 3\zeta)^{1/3}. \tag{4.13}$$

Hence, $\varphi = K^{1/3} + O(\zeta)$ for $\zeta \to 0$. Matching this to the inner solution v using (3.13), we find that $K = \lambda^3$ and so

$$\varphi = (\lambda^3 - 3\zeta)^{1/3}. \tag{4.14}$$

Sharp-interface model. We can now derive a matching condition from (4.14) by transforming it back into the outer variables. From (4.11) we have

$$v = \chi(\lambda^3 - 3\,\delta V^\nu \ln\chi)^{1/3}, \qquad \text{where } \chi = \frac{(\boldsymbol{x}-\boldsymbol{r})\cdot\boldsymbol{\nu}}{\varepsilon} \tag{4.15}$$

so that

$$h = (\boldsymbol{x}-\boldsymbol{r})\cdot\boldsymbol{\nu}(\lambda^3 - 3V^\nu)^{1/3} + O(\delta). \tag{4.16}$$

The following sharp-interface model then results as the leading-order outer problem, the boundary conditions being found by matching

$$\nabla\cdot(h^3\nabla\triangle h) = 0 \qquad \text{in } \Omega, \tag{4.17}$$

$$\frac{\partial h}{\partial \nu} = (\lambda^3 - 3V^\nu)^{1/3}, \qquad h = 0, \qquad h^3\frac{\partial}{\partial\nu}\triangle h = 0 \qquad \text{on } \Gamma^-, \tag{4.18}$$

$$\frac{\partial h}{\partial \nu} = (\lambda^3 - 3V^\nu)^{1/3}, \qquad h = 0, \qquad h^3\frac{\partial}{\partial\nu}\triangle h = 0 \qquad \text{on } \Gamma^+. \tag{4.19}$$

4.2. Stationary-ridge solutions and their linear stability

The stationary-ridge solutions of the sharp-interface model are the same as for the sharp-interface model for the slip case, i.e. parabolas with maximum normalized to one, and support $[-s_0, s_0]$, as stated in (3.24), (3.25). Now we again perturb these solutions, including the boundaries of the support, with normal-modes perturbations,

$$s^\pm = \pm s_0 + \beta s_1^\pm(k)\,\mathrm{e}^{\hat\sigma\tau + \mathrm{i}ky}, \qquad h = h_0 + \beta h_1(x;k)\,\mathrm{e}^{\hat\sigma\tau+\mathrm{i}ky}, \tag{4.20}$$

with $0 < \beta \ll 1$. Note that $\hat\sigma$ corresponds to the time variable τ, i.e. the relation to the growth rate in the scales of section 2 is $\sigma = \delta\hat\sigma$.

We then obtain for $O(\beta)$ the following eigenvalue problem, where $' = \mathrm{d}/\mathrm{d}x$,

$$h_1'' - k^2 h_1 = 0, \qquad \text{for } -\frac{2}{\lambda} < x < \frac{2}{\lambda}, \tag{4.21}$$

$$h_1 \mp \lambda s_1^\pm = 0 \qquad \text{at } x = \pm\frac{2}{\lambda}, \tag{4.22}$$

$$h_1' - \frac{1}{2}\lambda^2 s_1^\pm = -\frac{\hat\sigma}{\lambda^2}s_1^\pm \qquad \text{at } x = \pm\frac{2}{\lambda}. \tag{4.23}$$

Note, that the eigenvalue appears only in the last boundary condition. The ODE (4.21) is easily solved and upon inserting the general solution into the boundary conditions one finds non-trivial solutions for h_1 and $s_1^\pm$ if $\hat\sigma$ is equal to one of the two values,

$$\hat\sigma_+ = \tfrac{1}{2}\lambda^3(\lambda - 2k\tanh(2k/\lambda)) \tag{4.24}$$

and

$$\hat\sigma_- = \tfrac{1}{2}\lambda^3(\lambda - 2k\coth(2k/\lambda)), \tag{4.25}$$

i.e. $\hat\sigma_\pm$ are the two eigenvalues. Note that for shear-thickening liquids a similar asymptotic result was found in [32].

In figure 7 we compare the leading eigenvalues in outer scales from the numerical results for the full model by solving the eigenvalue problem (3.33)–(3.36) as before and comparing with the asymptotic values $\hat\sigma_+$ and $\hat\sigma_-$. Note here that the eigenvalues σ from section 2 have been rescaled appropriately with δ to match the scaling used for $\hat\sigma_\pm$. We find as $\varepsilon \to 0$ in figure 7 (right) that the numerical results approach the asymptotic value near the cut-off (neutrally stable) wavenumber k_c. In particular, the cut-off wavenumbers for the numerical results converge to the zero crossing of the asymptotic curve. In order to capture the linear stability behaviour for small wave numbers, we have to investigate the long-wave limit.

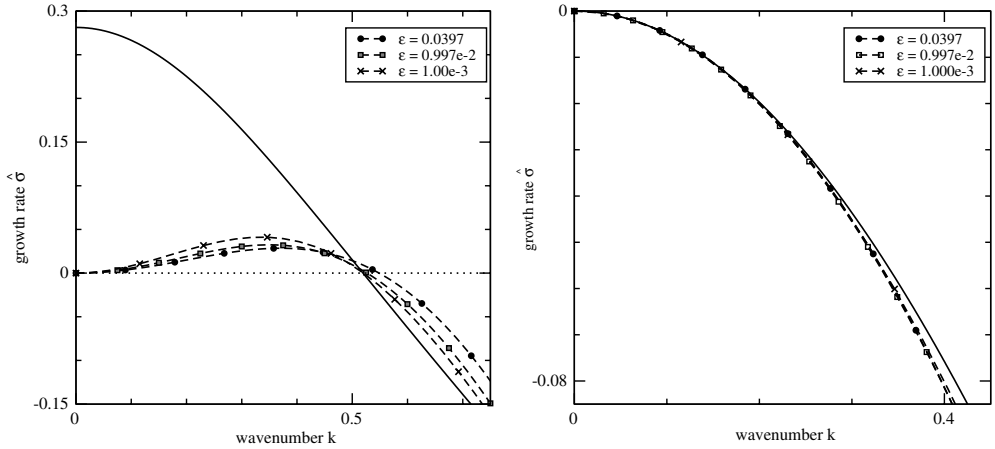

Figure 7. Here we show the dominant eigenvalue for the no-slip case (left) in outer scales (see (4.20) and (4.3)). The dashed lines with symbols show the results for the full model for different values of ε as indicated by the legend. The solid lines show the asymptotic results, using the eigenvalue $\hat{\sigma}_+$. The second (non-positive) eigenvalue for the no-slip case, in outer scales, compared with the asymptotic result $\hat{\sigma}_-$. The agreement of full and asymptotic model is quite good, in particular for longer wavelengths.

The long-wave limit. The previous asymptotic treatment assumes that the contact-line movement in the no-slip case is slow compared with the evolution of the solution in the bulk. This is encapsulated by the scaling of the time (τ) derivatives with δ, which is a (logarithmically) small quantity in terms of ϵ. Deviations of the ridge shape from the solution to Laplace's equation that vary on an order one spatial scale evolve on an order one scale of the original time variable t and rapidly decay before the contact-line movement sets in. As a result, the ridge achieves a quasistationary form and remains there even as the the contact line evolves. This is not true, however, for sufficiently long wave variations in the ridge (which accompany long-wave perturbations of the contact line). These can change on the same slow time scale τ as the contact-line motion, so the dynamics of the two no longer decouple. Consider therefore long wavelength perturbations of the ridge that vary on an order one scale of a new variable $\hat{y}$, given by $y = \hat{y}/\delta^{1/2}$. Introducing this scaling but keeping τ and x as before, we obtain, in place of (4.5), the equation

$$\delta h_\tau - (h^3 p_x)_x - \delta(h^3 p_{\hat{y}})_{\hat{y}} = 0, \qquad \text{where } p = -h_{xx} - \delta h_{yy} + \varepsilon^{-1}\Phi'(h/\varepsilon), \tag{4.26}$$

so that in this case to leading order

$$h^3 p_x = c(\hat{y}, \tau). \tag{4.27}$$

The boundary conditions $h^3 p_x = 0$ on Γ_1 and Γ_2 imply that $c(\hat{y}, \tau) = 0$ and $p = p(\hat{y}, \tau)$. Since, to leading order, $p = -h_{xx}$, integrating twice from s_- to s_+ yields the parabolic solution

$$h = -\tfrac{1}{2} p(\hat{y}, \tau)(x - s^-)(x - s^+). \tag{4.28}$$

Mass conservation leads to

$$\frac{\partial}{\partial \tau}\left[p \int_{s_-}^{s^+} (x^2 - (s^- + s^+)x + s^- s^+)\, \mathrm{d}x \right] = \frac{1}{4} \int_{s_-}^{s^+} \frac{\partial}{\partial \hat{y}} \left((x - s^-)^3 (x - s^+)^3 p^3 \frac{\partial p}{\partial \hat{y}} \right) \mathrm{d}x \tag{4.29}$$

and hence

$$\frac{\partial}{\partial\tau}[(s^+-s^-)^3p] = \frac{3}{1120}\frac{\partial}{\partial\hat{y}}\left[(s^+-s^-)^7\frac{\partial p^4}{\partial\hat{y}}\right]. \tag{4.30}$$

As the boundary conditions on (4.30) we find by matching to the inner solution that

$$s_\tau^\pm = \pm\tfrac{1}{3}(\mp h_x^3-\lambda^3).$$

Inserting (4.28) for h yields

$$s_\tau^\pm = \pm\tfrac{1}{3}\left(\tfrac{1}{8}(s^+-s^-)^3p^3-\lambda^3\right). \tag{4.31}$$

For the base state we note that $s^\pm$ and p are independent of y and t, and using (4.31), we get

$$h_0 = -\tfrac{1}{2}p_0(x-s_0^-)(x-s_0^+), \qquad p_0(s_0^+-s_0^-)=2\lambda. \tag{4.32}$$

If we put the origin in x-direction in the middle of the parabolic ridge, then $s_0^+ = s_0$ and $s_0^- = -s_0$ and

$$h_0 = -\tfrac{1}{2}p_0(x^2-s_0^2), \qquad p_0s_0=\lambda. \tag{4.33}$$

Taking $\max h_0 = s_0^2p_0/2 = 1$ yields the base state

$$s_0 = \frac{2}{\lambda}, \qquad p_0 = \frac{\lambda^2}{2}. \tag{4.34}$$

Perturbation about this base state via

$$s^+ = s_0+\beta s_1^+(\hat{y},\tau)+O(\beta^2), \qquad s^- = -s_0+\beta s_1^-(\hat{y},\tau)+O(\beta^2), \tag{4.35}$$

$$p = p_0+\beta p_1(\hat{y},t)+O(\beta^2), \tag{4.36}$$

yields at $O(\beta)$ the equations

$$s_0^2p_0(s_1^+-s_1^-)_\tau + s_0^3p_{1\tau} = \tfrac{4}{35}s_0^7p_0^3p_{1\hat{y}\hat{y}}, \tag{4.37}$$

$$s_{1\tau}^\pm = \pm\left(p_0^2s_0^3p_1+\tfrac{1}{2}p_0^3s_0^2(s_1^+-s_1^-)\right). \tag{4.38}$$

A change in variable

$$s_1 := \tfrac{1}{2}(s_1^+-s_1^-), \qquad m_1 := \tfrac{1}{2}(s_1^++s_1^-) \tag{4.39}$$

simplifies the system to

$$3s_0^2p_0s_{1\tau}+s_0^3p_{1\tau} = \tfrac{6}{35}s_0^7p_0^3p_{1\hat{y}\hat{y}}, \tag{4.40}$$

$$s_{1\tau} = p_0^2s_0^3p_1+p_0^3s_0^2s_1, \tag{4.41}$$

$$m_{1\tau}=0. \tag{4.42}$$

Hence using (4.34)

$$s_{1\tau}+\frac{4}{3\lambda^3}p_{1\tau} = \frac{16}{35\lambda}p_{1yy}, \qquad s_{1\tau} = \lambda^2\left(\frac{2}{\lambda}p_1+\frac{\lambda^2}{2}s_1\right). \tag{4.43}$$

The normal modes ansatz

$$s_1(\hat{y},\tau) = a\mathrm{e}^{\hat{\sigma}\tau+\mathrm{i}\hat{k}\hat{y}} \qquad \text{and} \qquad p_1(\hat{y},\tau) = b\mathrm{e}^{\hat{\sigma}\tau+\mathrm{i}\hat{k}\hat{y}} \tag{4.44}$$

yields then the following quadratic equation for the growth rate $\hat{\sigma}$

$$\hat{\sigma}^2+\left(\lambda^4+\tfrac{12}{35}\lambda^2\hat{k}^2\right)\hat{\sigma}-\tfrac{6}{35}\lambda^6\hat{k}^2=0. \tag{4.45}$$

A comparison of the larger of the two solutions of (4.45) with the results for the full model in section 2 is shown in figure 8, in terms of $\hat{k}$ and $\hat{\sigma}$. Indeed, the agreement is good for small wave numbers and improves as ε is decreased. The other solution of (4.45) tends to a non-zero $O(1)$ for $k\to 0$, hence does not correspond to any of the two eigenvalues of the full problem we investigate here, which are both neutrally stable for $k=0$.

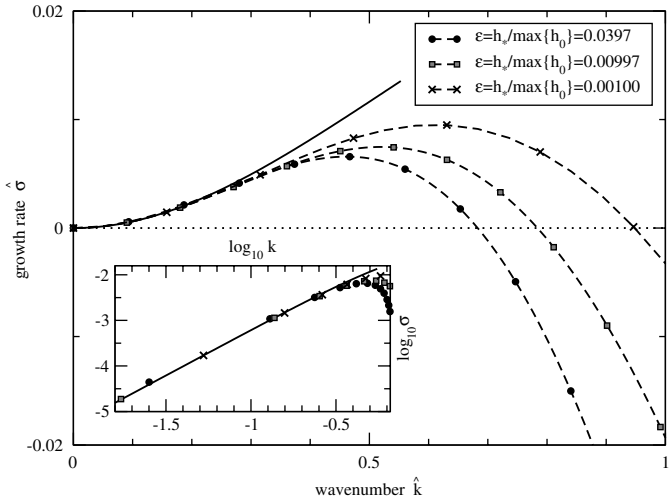

Figure 8. Here we show the dominant eigenvalue for the no-slip case and the larger solution of (4.45). Note that we show $\hat{\sigma}$, i.e. the eigenvalues are scaled as in figure 7, but the wavenumber is now in the scalings for the long-wave approximation, $\hat{k} = k/\delta^{1/2}$. The inset is a double logarithmic plot of part of the larger figure.

Composite solution. Finally, we can also compare the asymptotic composite solution with the solution to the eigenvalue problem for the full problem (3.33)–(3.36). For this we focus on the first eigenvalue. Equation (4.24) yields an approximation of $\sigma = \delta\hat{\sigma}$ for $k = O(1)$, while (4.45) is valid if $\hat{k} = O(1)$. Expanding the former at $k = 0$ yields

$$\sigma = \delta\hat{\sigma} \sim \delta\left(\tfrac{1}{2}\lambda^4 - 2\lambda^2 k^2 + \tfrac{8}{3}k^4\right). \tag{4.46}$$

Expanding the solution of (4.45) at $\hat{k} = \infty$ we find after replacing $\hat{k}$ by $k/\delta^{1/2}$

$$\sigma = \delta\hat{\sigma} \sim \tfrac{1}{2}\delta\lambda^4 - \tfrac{35}{16}\delta\frac{\lambda^6}{k^2}. \tag{4.47}$$

Hence $\delta\lambda^4/2$ is the common part of both expansions. We therefore construct the composite solution by multiplying the solution of (4.45) (times δ) with the expression (4.24) (times δ) and then dividing by the common part. A comparison of this composite solution with our numerical results for the full model can be seen in figure 9.

5. Conclusion

In this paper we have derived sharp-interface models for a stationary ridge from the lubrication models with mobilities h^3 and h^2, corresponding to the no-slip boundary condition at the liquid/solid interface and a condition for large slippage, respectively. For this simple situation we were able to derive, in the no-slip case, analytical expressions for the dispersion relations that characterize the linear stability of the three-phase contact line. The instability mechanism is closely related to Rayleigh–Plateau instability of a free cylinder of fluid—as the peristaltic pertubations grow, the ridge can be expected to break up and eventually form droplets with circular contact lines in order to reduce its surface area. Our approach can be generalized to the situation of a dewetting ridge, the major differences being that the base state is not stationary and non-symmetrical due to the non-symmetrical form of the boundary conditions.

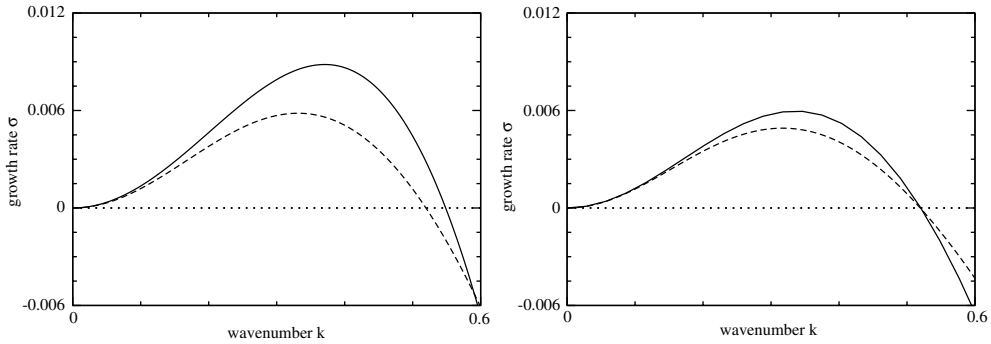

Figure 9. Here we compare the asymptotic composite solution (- - - -) with the eigenvalue problem for the full problem i.e. (2.4)–(2.5) with $n = 3$ (——) for $\varepsilon = 0.0397$ (left) and $\varepsilon = 1.000 \times 10^{-3}$ (right). The wavenumbers and growth rates are scaled as in section 2.

Acknowledgments

AM acknowledges support via DFG Grant MU 1626/3-1 and by the DFG research center MATHEON, Berlin. JRK gratefully acknowledges the hospitality of the WIAS, where this work was initiated.

Appendix A. Transformation to inner variables

For completeness we include here the transformation formulae for the inner region.

Suppose $\tilde{w}$ is a quantity defined in the inner coordinates (s, χ, t). Then its derivatives are related to the derivatives of the corresponding quantity w in outer coordinates via the invertible transformation matrix

$$M = \begin{pmatrix} & & 0 \\ & Q & 0 \\ x_t & y_t & 1 \end{pmatrix}, \qquad \text{where } Q = \begin{pmatrix} x_s & y_s \\ x_\chi & y_\chi \end{pmatrix}, \tag{A.1}$$

by

$$\begin{pmatrix} \tilde{w}_s \\ \tilde{w}_\chi \\ \tilde{w}_t \end{pmatrix} = M \begin{pmatrix} w_x \\ w_y \\ w_t \end{pmatrix}. \tag{A.2}$$

Since s is arclength, we have

$$r_{1s}^2 + r_{2s}^2 = 1, \qquad r_{1s} r_{1ss} + r_{2s} r_{2ss} = 0, \qquad \kappa(s,t) = r_{1s} r_{2ss} - r_{2s} r_{1ss} \tag{A.3}$$

and the (two-dimensional) Frenet–Serret formulae

$$\boldsymbol{t}_s = \kappa \boldsymbol{\nu}, \qquad \boldsymbol{\nu}_s = -\kappa \boldsymbol{t}, \tag{A.4}$$

so that

$$r_{1ss} = -\kappa r_{2s}, \qquad r_{2ss} = \kappa r_{1s}. \tag{A.5}$$

Hence

$$\boldsymbol{x}_s = (1 - \varepsilon\chi\kappa)\boldsymbol{t}, \qquad \boldsymbol{x}_\chi = \varepsilon\boldsymbol{\nu}, \qquad \det Q = \varepsilon(1 - \varepsilon\chi\kappa). \tag{A.6}$$

Now we can express the derivatives with respect to the outer variables of a quantity w in terms of the inner variables by

$$\begin{pmatrix} w_x \\ w_y \\ w_t \end{pmatrix} = \begin{pmatrix} \mathrm{Q}^{-1} & 0 \\ -\boldsymbol{x}_t \cdot \mathrm{Q}^{-1} & 1 \end{pmatrix} \begin{pmatrix} \tilde{w}_s \\ \tilde{w}_\chi \\ \tilde{w}_t \end{pmatrix}$$
$$\sim \begin{pmatrix} r_{1s}(1+\varepsilon\chi\kappa) & -\varepsilon^{-1} r_{2s} & 0 \\ r_{2s}(1+\varepsilon\chi\kappa) & \varepsilon^{-1} r_{1s} & 0 \\ -V^t(1+\varepsilon\chi\kappa) & -\varepsilon^{-1} V^\nu & 1 \end{pmatrix} \begin{pmatrix} \tilde{w}_s \\ \tilde{w}_\chi \\ \tilde{w}_t \end{pmatrix} \tag{A.7}$$

as $\varepsilon \to 0$, where we have used the approximation $1/(1-\varepsilon\chi\kappa) = 1 + \varepsilon\chi\kappa + O(\varepsilon^2)$.

The second derivatives then transform as follows:

$$w_{xx} \sim \varepsilon^{-2} r_{2s}^2 \tilde{w}_{\chi\chi} - \varepsilon^{-1}[\kappa r_{1s}^2 \tilde{w}_\chi + 2 r_{1s} r_{2s} \tilde{w}_{s\chi}] + r_{1s}^2 \tilde{w}_{ss}$$
$$- 2\kappa r_{1s} r_{2s} \tilde{w}_s - \chi\kappa[\kappa r_{1s}^2 \tilde{w}_\chi + 2 r_{1s} r_{2s} \tilde{w}_{s\chi}] \tag{A.8}$$

$$w_{yy} \sim \varepsilon^{-2} r_{1s}^2 \tilde{w}_{\chi\chi} - \varepsilon^{-1}[\kappa r_{2s}^2 \tilde{w}_\chi - 2 r_{1s} r_{2s} \tilde{w}_{s\chi}] + r_{2s}^2 \tilde{w}_{ss}$$
$$+ 2\kappa r_{1s} r_{2s} \tilde{w}_s - \chi\kappa[\kappa r_{2s}^2 \tilde{w}_\chi - 2 r_{1s} r_{2s} \tilde{w}_{s\chi}] \tag{A.9}$$

$$w_{xy} \sim -\varepsilon^{-2} r_{1s} r_{2s} \tilde{w}_{\chi\chi} - \varepsilon^{-1}[\kappa r_{1s} r_{2s} \tilde{w}_\chi + (r_{2s}^2 - r_{1s}^2)\tilde{w}_{s\chi}]$$
$$+ r_{1s} r_{2s} \tilde{w}_{ss} - \kappa(r_{2s}^2 - r_{1s}^2)\tilde{w}_s - \chi\kappa[\kappa r_{1s} r_{2s} \tilde{w}_\chi + (r_{2s}^2 - r_{1s}^2)\tilde{w}_{s\chi}] \tag{A.10}$$

$$\triangle w \sim \varepsilon^{-2} \tilde{w}_{\chi\chi} - \varepsilon^{-1}\kappa \tilde{w}_\chi + \tilde{w}_{ss} - \chi\kappa^2 \tilde{w}_\chi. \tag{A.11}$$

Appendix B. Higher order approximation for the slope

Given that the leading order expressions in the no-slip case are nominally only logarithmically accurate in ε, we record here, in part for future reference, the first correction term and then note its implications for the current problem.

Higher order in δ approximations for λ (the slope used in the main part of the paper will be denoted here by λ_0) may be achieved by starting with equation (4.4)

$$\delta h_t + \nabla \cdot (h^3 \nabla \cdot [\triangle h - \varepsilon^{-1}\Phi'(h/\varepsilon)]) = 0. \tag{B.1}$$

In inner scales, keeping $O(\delta)$ terms, we obtain with $h = \varepsilon g$

$$\delta \dot{s} g_\chi \sim (g^3(g_{\chi\chi} - \Phi'(g))_\chi)_\chi. \tag{B.2}$$

Integrating yields

$$\delta \dot{s}(g - h_\infty) \sim g^3(g_{\chi\chi} - \Phi'(g))_\chi, \qquad \text{where } h_\infty \sim 1. \tag{B.3}$$

Let $g \sim g_0 + \delta g_1$, then to leading order in δ we find

$$\tfrac{1}{2} g_{0\chi}^2 = \Phi(g_0) - \Phi(1), \qquad \text{so that } \lambda_0 = \sqrt{2(-\Phi(1))}, \tag{B.4}$$

or, if we set

$$g_{0\chi} = -\Psi(g_0), \qquad \text{we find } \lambda_0 = \Psi(\infty). \tag{B.5}$$

To next order we get

$$\dot{s}(g_0 - 1) = g_0^3(g_{1\chi\chi} - \Phi''(g_0)g_1)_\chi. \tag{B.6}$$

Integrating this yields

$$g_{1\chi\chi} - \Phi''(g_0)g_1 = \dot{s}\int_{-\infty}^{\chi} \frac{g_0 - 1}{g_0^3} \mathrm{d}\chi = \dot{s}\int_{g_0}^{\infty} \frac{g-1}{g^3\Psi(g)} \mathrm{d}g \tag{B.7}$$

If we denote

$$\Omega(g_0) = \int_{g_0}^{\infty} \frac{g-1}{g^3\Psi(g)}\mathrm{d}g, \tag{B.8}$$

then, making use of (B.4), we obtain the equation

$$g_{0\chi}g_{1\chi\chi} - g_1 g_{0\chi\chi\chi} = \dot{s}\Omega(g_0)g_{0\chi} \tag{B.9}$$

Integrating once we find

$$g_{0\chi}g_{1\chi} - g_1 g_{0\chi\chi} = -\dot{s}\int_{\chi}^{\infty} \Omega(g_0)g_{0\chi}\,\mathrm{d}\chi = \dot{s}\int_1^{g_0} \Omega(g)\,\mathrm{d}g. \tag{B.10}$$

Thus

$$-\lambda_0 g_{1\chi} \sim \dot{s}\frac{\ln(\lambda_0\chi)}{\lambda_0} + \dot{s}\int_1^{g_0} \Omega - \frac{1}{\lambda_0 g}\,\mathrm{d}g \qquad \text{as } \chi \to -\infty. \tag{B.11}$$

If we now let $\lambda \sim \lambda_0 + \delta\lambda_1$, then we find

$$\lambda_1 = \dot{s}\frac{\ln(\lambda_0) - 1}{\lambda_0^2} + \frac{\dot{s}}{\lambda_0}\int_1^{\infty} \Omega - \frac{1}{\lambda_0 g}\,\mathrm{d}g. \tag{B.12}$$

The most important implication of this in the current context follows from the fact that λ_1 is proportional to $\dot{s}$. Because our base state has $\dot{s} = 0$, the contributions of such correction terms to the stability analysis are in consequence significantly less important than they would be in other contexts. We anticipate that this is reflected in the accuracy of asymptotics illustrated in figure 9.

References

[1] Huppert H 1982 Flow and instability of a viscous current down a slope *Nature* **300** 427–9
[2] Silvi N and Dussan E B V 1985 On the rewetting of an inclined solid surface by a liquid *Phys. Fluids* **28** 5–7
[3] Bertozzi A L and Brenner M P 1997 Linear stability and transient growth in driven contact lines *Phys. Fluids* **9** 530–9
[4] Troian S M, Herbolzheimer E, Safran S A and Joanny J F 1989 Fingering instabilities of driven spreading films *Europhys. Lett.* **10** 25–30
[5] Hocking L M and Miksis M J 1993 Stability of a ridge of fluid *J. Fluid Mech.* **247** 157–77
[6] Cazabat A M, Heslot F, Troian S M and Carles P 1990 Finger instability of thin spreading films driven by temperature gradients *Nature* **346** 824–6
[7] Brzoska J B, Brochard-Wyart F and Rondelez F B 1992 Exponential growth of fingering intabilities of spreading films under horizontal thermal gradients *Europhys. Lett.* **19** 97–102
[8] Garnier N, Grigoriev R O and Schatz M F 2003 Optical manipulation of microscale fluid flow *Phys. Rev. Lett.* **91** 054501
[9] Kataoka D E and Troian S M 1997 A theoretical study of instabilities at the advancing front of thermally driven coating films *J. Colloid Interface Sci.* **192** 350–62
[10] Bertozzi A L, Münch A, Fanton X and Cazabat A M 1998 Contact line stability and 'undercompressive shocks' in driven thin film flow *Phys. Rev. Lett.* **81** 5169–72
[11] López P G, Bankoff S G and Miksis M J 1996 Non-isothermal spreading of a thin liquid film on an inclined plane *J. Fluid Mech.* **11** 1–39
[12] Münch A and Wagner B A 1999 Numerical and asymptotic results on the linear stability of a thin film spreading down a slope of small inclination *Euro. J. Appl. Math.* **10** 297–318
[13] Seemann R, Herminghaus S and Jacobs K 2001 Dewetting patterns and molecular forces: a reconciliation *Phys. Rev. Lett.* **86** 5534–7
[14] Seemann R, Herminghaus S and Jacobs K 2001 Gaining control of pattern formation of dewetting films *J. Phys.: Condens. Matter* **13** 4925–38
[15] Konnur R, Kargupta K and Sharma A 2000 Instability and morphology of thin liquid films on chemically heterogeneous substrates *Phys. Rev. Lett.* **84** 931–4
[16] Reiter G 1992 Dewetting of thin polymer films *Phys. Rev. Lett.* **68** 75–8

[17] Reiter G, Sharma A, Casoli A, David M-O, Khanna R and Auroy P 1999 Thin film instability induced by long-range forces *Langmuir* **15** 2551–8
[18] Sharma A and Khanna R 1998 Pattern formation in unstabile thin liquid films. *Phys. Rev. Lett.* **81** 3463–6
[19] Sharma A and Khanna R 1999 Pattern formation in unstable thin liquid films under influence of antagonistic short- and long-range forces *J. Chem. Phys.* **110** 4929–36
[20] Xie R, Karim A, Douglas J F, Han C C and Weiss R A 1998 Spinodal dewetting of thin polymer films *Phys. Rev. Lett.* **81** 1251–4
[21] Neto C and Jacobs K 2004 Dynamics of hole growth in dewetting polystyrene films *Physica* A **339** 66–71
[22] Redon C, Brzoska J B and Brochard-Wyart F 1994 Dewetting and slippage of microscopic polymer films *Macromolecules* **27** 468–71
[23] Redon C, Brochard-Wyart F and Rondelez F 1991 Dynamics of dewetting *Phys. Rev. Lett.* **66** 715–8
[24] Brochard-Wyart F, de Gennes P-G, Hervert H and Redon C 1994 Wetting and slippage of polymer melts on semi-ideal surfaces *Langmuir* **10** 1566–72
[25] Jacobs K, Seemann R, Schatz G and Herminghaus S 1998 Growth of holes in liquid films with partial slippage *Langmuir* **14** 4961–3
[26] Reiter G and Sharma A 2001 Auto-optimization of dewetting rates by rim instabilities in slipping polymer films *Phys. Rev. Lett.* **87** 166103
[27] Münch A and Wagner B 2005 Contact-line instability of dewetting thin films *Physica* D **209** 178–90
[28] Münch A 2004 Fingering instability in dewetting films induced by slippage Matheon *Preprint* 123
[29] Münch A, Wagner B and Witelski T P 2005 Lubrication models for small to large slip-lengths *J. Eng. Math.* **53** 359–83
[30] Münch A 2005 Dewetting rates of thin liquid films *J. Phys.: Condens. Matter* **17** S309–18
[31] Ghatak A, Khanna R and Sharma A 1999 Dynamics and morphology of holes in dewetting of thin films *J. Colloid Interface Sci.* **212** 483–94
[32] Flitton J C and King J R 2005 Surface-tension-driven dewetting of Newtonian and power-law fluids *J. Eng. Math.* **50** 241–66
[33] Glasner K B 2005 Variational models for moving contact lines and the quasi-static approximation *Euro. J. Appl. Math.* **16** 1–28
[34] Glasner K B 2005 A boundary integral formulation of quasi-steady fluid wetting *J. Comput. Phys.* **207** 529–41
[35] King J R and Bowen M 2001 Moving boundary problems and non-uniqueness for the thin film equation *Eur. J. Appl. Math.* **12** 321–56
[36] King J R 2001 The spreading of power law fluids *Proc. IUTAM Symposium on Free Surface Flows (Birmingham, UK, 2000)* ed A C King and Y D Shikmurzaev (Dordrecht: Kluwer) pp 153–60